AIAA SciTech Forum
7-11 January 2019, San Diego, California
AIAA Scitech 2019 Forum

10.2514/6.2019-2228

Shape Continuum Sensitivity Analysis using ASTROS and CAPS

Robert A. Canfield[1], Suood Alnaqbi,[2]
Virginia Tech, Blacksburg, VA 24061 USA

Ryan J. Durscher,[3] Dean E. Bryson,[4] and Raymond M. Kolonay[5]
Air Force Research Laboratory, Wright-Patterson AFB, OH 45433 USA

Continuum Sensitivity Analysis (CSA) is an analytic method that may compute derivatives with respective to shape variables, which may be formulated in fundamentally different ways. The boundary velocity formulation of CSA presented here enables an element-agnostic implementation that hinges upon post-processing of output from the analysis solver using a nonintrusive spatial gradient reconstruction (SGR) technique. SGR has been implemented as a module in the Automated Structural Optimization System (ASTROS). SGR provides the spatial derivatives used in conjunction with geometric sensitivity, also known as the design velocity, to form the convective term of CSA boundary conditions. The Computational Aircraft Prototype Syntheses (CAPS) program represents parametric associative geometry of solids and surfaces that conveniently provides the geometric sensitivity essential to forming the CSA boundary conditions. A procedure is described here that uses CAPS to provide the surface geometry, geometric sensitivity, and mesh of a finite element model for which ASTROS is used to perform SGR of the structural analysis output and then perform CSA. Results from a simple beam bending model in two- and three-dimensional space verify, against an analytic solution, the implementation of shape CSA using ASTROS and CAPS.

I. Introduction

Conceptual design of aircraft includes definition of the outer moldline of the vehicle being designed, which may be parameterized by shape design variables. The outer moldline, in turn, governs structural layout, dictating configuration of structural components such as spars, ribs, skins, and stiffeners. Generating discrete models of various fidelity for repeated multidisciplinary analysis and optimization (MDAO) is a challenging process that often limits the design process. Parametric associative geometry as the starting point has long been recognized as a critical step in automating MDAO. The Computational Aircraft Prototype Syntheses (CAPS) program, which is a part of the Engineering Sketch Pad (ESP), combines "proven computational geometry, meshing, and analyses model generation techniques into a complete browser-based, client-server environment that is accessible to the entire design team of an aerospace vehicle. CAPS links analysis and meshing disciplines to any ESP geometry model via dynamically-loadable Analysis Interface Module (AIM) plugins." [1] Dannenhoffer and Haimes have demonstrated the usefulness of ESP as a tool to provide geometric sensitivity that is commonly needed, at some level, by all methods that compute shape derivatives, including adjoint solvers found in such computational fluid dynamics (CFD) solvers as CART3D and FUN3D [2]. Haimes and Dannenhoffer have focused on the process of automating adaptive mesh generation starting from the parametric associative geometry in ESP and CAPS [3]. Aside from adaptive meshing, geometric sensitivity, that is the derivatives of grid point locations in a mesh with respect to the shape variables that parameterize the geometry, are needed to drive the solution for derivatives of the solution with respect to the shape variables, whether it be a direct or adjoint sensitivity method. The authors have built into the CAPS AIM for ASTROS [4] and NASTRAN [5] an interface definition for the geometric sensitivity of grid points with respect to geometric shape parameters needed for the semi-analytic shape sensitivity method in NASTRAN and a new analytic shape sensitivity method added as an ASTROS module.

The Automated Structural Optimization System (ASTROS) was developed for sizing aerospace structures [4]. Its design variables were limited to controlling the sizes of one- and two-dimensional \ elements. Although it has a

[1] Professor and Assistant Head, Kevin T. Crofton Department of Aerospace and Ocean Engineering, Associate Fellow
[2] Undergraduate Research Assistant, Kevin T. Crofton Department of Aerospace and Ocean Engineering
[3] Research Aerospace Engineer, Multidisciplinary Science and Technology Center AFRL/RQVC
[4] Research Aerospace Engineer, Multidisciplinary Science and Technology Center AFRL/RQVC
[5] Director, Multidisciplinary Science and Technology Center AFRL/RQVC, Associate Fellow

hexahedral solid element, neither its grid points nor grid points of the other elements are controllable by design variables. Nevertheless, its modular architecture allows users to add such capability, including the addition of new bulk data input. In the capability developed here, input for defining shape design variables that control grid points was defined by replicating NASTRAN's DVGRID bulk data entry. NASTRAN, on the hand, features design sensitivity analysis for which users may define design variables that control grid points by way of input of that is sometimes called the design velocity. Although NASTRAN has options to automate the computation of design velocity by way of auxiliary models, they are not geometric models. For general geometry-based finite element models (FEMs), the user may input design velocity, which CAPS can now provide for NASTRAN or ASTROS for any of a user's geometric parameters. Other geometric data needed to formulate shape sensitivity loading conditions, which are not inherent to the FEM, are the surface normals and their material derivatives where boundary surfaces change orientation with a change in shape variable. NASTRAN defines an SNORM bulk data entry for the user to input surface normal vectors, but once again they are not inherent to the FEM but rather must come from the geometry parameterization. The SNORM has been replicated in ASTROS and a new SNORMDT bulk data entry (missing in NASTRAN) has been created in ASTROS. The CAPS AIM generates them from the geometry and geometric sensitivity.

Whereas NASTRAN uses design velocity throughout the domain to drive finite differences of element matrices, which are assembled into the right-side sensitivity load for its semi-analytic sensitivity analysis, we have implemented an analytic sensitivity computation in ASTROS. A taxonomy of sensitivity methods is depicted in Fig. 1. The boundary-velocity formulation of continuum sensitivity analysis (BV-CSA) computes local derivatives throughout the domain driven by sensitivity loads applied on the boundaries. Hence, its right-side sensitivity loads require design velocity only on the boundaries. In addition to design velocity (geometric sensitivity) on the boundaries, CSA calls for spatial derivatives of the FEM solution on the boundary. Early on in the literature, the relatively inaccurate spatial derivatives of the FEM solution on the boundary of low-order FEMs inhibited the use of BV-CSA [6]. More recently Liu and Canfield [7] demonstrated the viability of BV-CSA for higher-order *p*-elements. Subsequently, Cross and Canfield [8] demonstrated that, following Zienkiewicz and Zhu [9], spatial gradient reconstruction (SGR) from multi-layer patches of elements could recover the rate of convergence of the FEM analysis in BV-CSA. Input bulk data for SGR patches have been defined in ASTROS. CAPS now has the ability to automatically generate SGR patches of elements for ASTROS on geometric boundary surfaces that change shape.

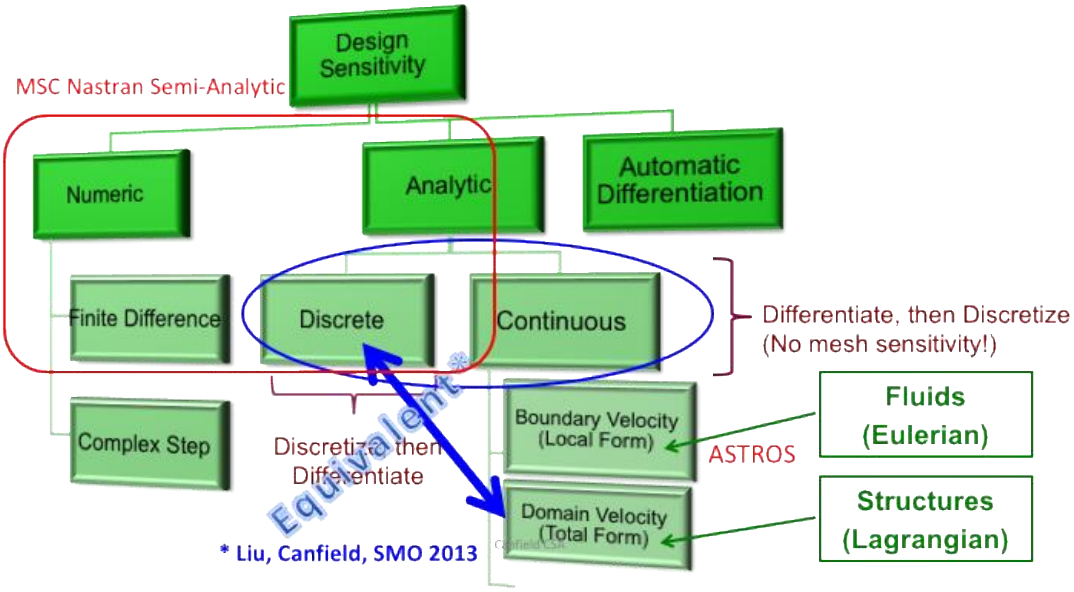

Figure 1. Taxonomy of Sensitivity Analysis Methods

II. Technical Approach

The approach is to differentiate the governing equations to arrive at a system of integro-differential *continuum sensitivity equations* (CSEs). To solve these CSEs, one first differentiates the boundary conditions to specify the sensitivity boundary conditions. Then, the system of CSE's may be discretized and solved. Whereas the CSA boundary conditions must be derived using the material (total) derivative, it is advantageous to derive the CSE system using local derivatives, known as the *boundary velocity formulation* CSA. A chief benefit is that the geometric sensitivity, known as the domain design velocity, or mesh sensitivity of discretized systems, is not required to solve for the local derivatives with respect to shape variables. Furthermore, unlike discrete sensitivity analysis (DSA), differentiation of the discrete system (Jacobian or tangent stiffness) matrix is avoided. The proposed nonintrusive approach, using SGR, enables shape sensitivity using existing analysis codes executed non-intrusively in a "black box" manner. A flow chart for the BV-CSA-SGR procedure is shown in Fig. 2. The theoretical background and technical approach for SGR-based shape BV-CSA, documented in detail in references [10-15], is summarized next. Sample input data and their bulk data descriptions are shown in figures of the Appendix.

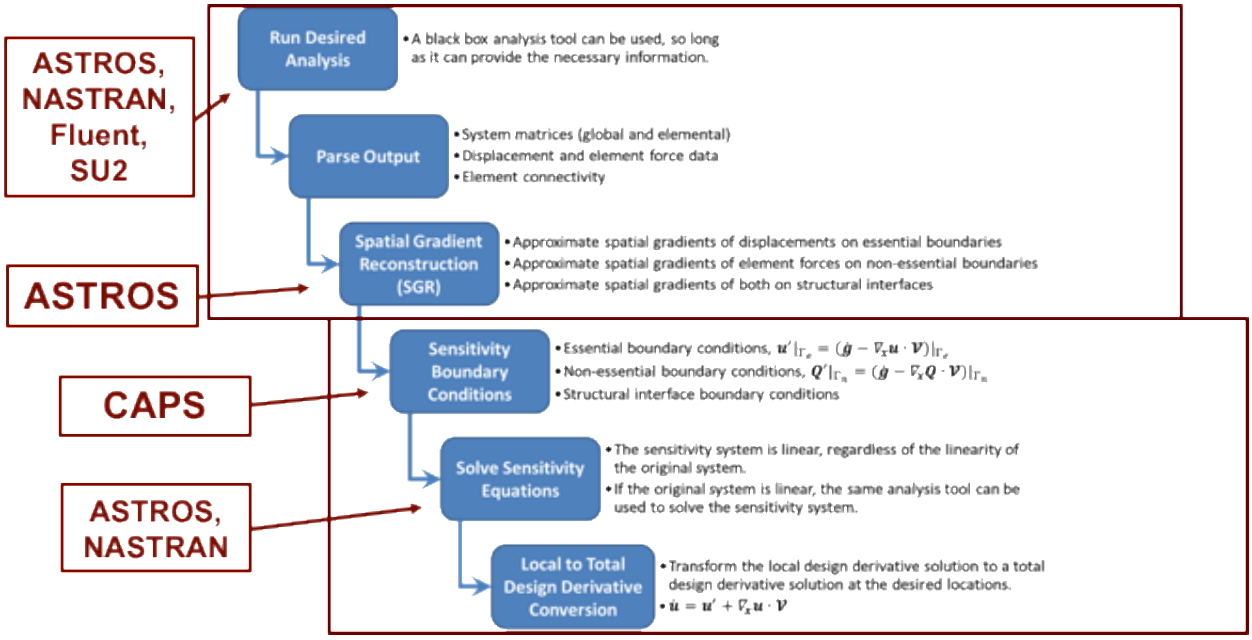

Figure 2. Flow Chart of BV-CSA implemented in ASTROS with SGR

The CSA method commences with continuous equations in terms of state variables before the system of equations is discretized. Consider the following general boundary value system defined in a domain Ω with a boundary Γ

$$\mathcal{A}(\boldsymbol{u}) - \boldsymbol{f}(\boldsymbol{x}, t; b) = 0 \quad \text{on} \quad \Omega \tag{1}$$

$$\mathcal{B}(\boldsymbol{u}) = \boldsymbol{g}(\boldsymbol{x}, t; b) \quad \text{on} \quad \Gamma \tag{2}$$

for which we seek a solution for the vector of dependent (state) variables $\boldsymbol{u}(\boldsymbol{x}, t; b)$ are functions of the spatial and temporal independent coordinates, $\boldsymbol{x}$ and t, respectively and depend implicitly on design variable b. $\mathcal{A}$ and $\mathcal{B}$ are differential or integro-differential operators. Essential (geometric) boundary conditions specified on Γe, and non-essential (natural) boundary conditions specified on Γn of this boundary value problem. The general analysis Eqs. (1) and BCs (2) may apply to a fluid domain Ω_f or structure domain Ω_s.

For shape sensitivity, Eqs. (1–2) are differentiated with respect to b and may be solved for local derivative $\partial \boldsymbol{u}/\partial b$, expressed at the highest level, as

$$\bar{\mathcal{A}}(\boldsymbol{u}'; \boldsymbol{u}) = \boldsymbol{f}'(\boldsymbol{x}, t; b) \quad \text{on} \quad \Omega \tag{3}$$

subject to sensitivity boundary conditions.

$$\bar{\mathcal{B}}(\boldsymbol{u}'; \boldsymbol{u}) = \dot{\boldsymbol{g}}(\boldsymbol{x}, t; b) - \nabla \mathcal{B}(\boldsymbol{u}) \cdot \mathcal{V}(\boldsymbol{x}) \quad \text{on} \quad \Gamma \tag{4}$$

where for linear systems $\bar{\mathcal{A}} = \mathcal{A}$ and $\bar{\mathcal{B}} = \mathcal{B}$, but they generally are not the same for nonlinear systems. The total derivative of u with respect to design parameter b at a material point

$$\frac{D\boldsymbol{u}}{Db} = \frac{\partial \boldsymbol{u}}{\partial b} + \nabla \boldsymbol{u} \cdot \mathcal{V}(\boldsymbol{x}) \qquad \Longleftrightarrow \qquad \dot{\boldsymbol{u}} = \boldsymbol{u}' + \nabla \boldsymbol{u} \cdot \mathcal{V}(\boldsymbol{x}) \tag{5}$$

consists of the local derivative, $\boldsymbol{u}'$, and a convective term involving the inner product of the spatial gradient and design velocity. The latter accounts for how $\boldsymbol{u}$ changes as the material point moves in response to design variable changes, where $\nabla \boldsymbol{u}$ is the gradient of $\boldsymbol{u}$ with respect to the spatial coordinates, and $\mathcal{V}(\boldsymbol{x}) = \partial \boldsymbol{x}/\partial b$ is the geometric sensitivity or design velocity, which depends on the parameterization of the computational domain. Eq. (5) requires that the domain changes linearly with respect to the design parameter b as described by the following domain mapping $\boldsymbol{x}_b(\boldsymbol{x}, b) = \boldsymbol{x} + b\,\mathcal{V}(\boldsymbol{x})$, where $\boldsymbol{x}_b$ is the vector of perturbed coordinates. The spatial gradients appearing in Eqs. (5) and (6) were reconstructed using the SGR technique [8-9]. SGR was applied to get 2D and 3D spatial derivatives of displacements and stresses. As an example, for second-order SGR, the following second-order Taylor series expansion is used to solve the least-squares problem, where ϕ may represent a displacement component of $\boldsymbol{u}_s$ or a component of stress, such as σ_{xx}, or a velocity component of $\boldsymbol{u}_f$.

$$\begin{aligned}\phi(x+\Delta x,\ y+\Delta y,\ z+\Delta z) = {} & \phi(x,\ y,\ z) + \phi_{,x}\Delta x + \phi_{,y}\Delta y + \phi_{,z}\Delta z \\ & + \frac{1}{2}\phi_{,xx}\,(\Delta x)^2 + \frac{1}{2}\phi_{,yy}\,(\Delta y)^2 + \frac{1}{2}\phi_{,zz}\,(\Delta z)^2 \\ & + \phi_{,xy}\Delta x\Delta y + \phi_{,yz}\Delta y\Delta z + \phi_{,zx}\Delta z\Delta x\end{aligned} \tag{6}$$

III. Results

Timoshenko Beam Two-Dimensional Analytical Benchmark

Timoshenko's two-dimensional plane elasticity analytical solution [16] for a cantilever beam with shear deformation was used to verify the BV-CSA-SGR implementation in CAPS and ASTROS. Essential boundary conditions on the cantilever end and parabolic shear distribution at the free end are specified according to [17], as depicted in Fig. 3.

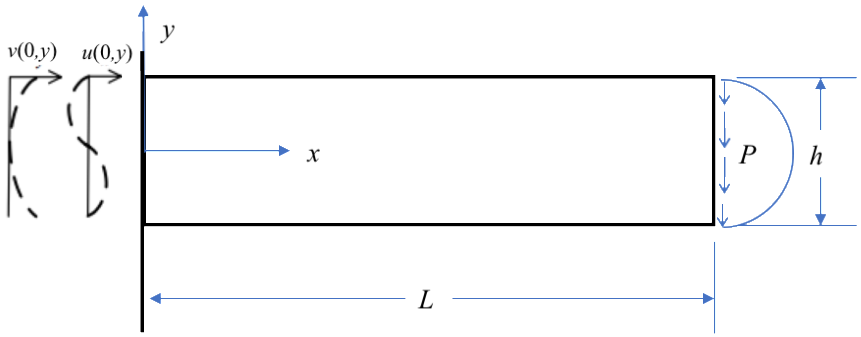

Figure 3. Timoshenko's two-dimensional cantilever beam coordinate system with enforced boundary displacement (left) and parabolic shear end load (right)

Timoshenko and Goodier [16] derived the analytic elasticity solution for bending of a two-dimensional rectangular cantilever beam loaded with a parabolically distributed transverse shear force at its free end. That elasticity solution may be differentiated with respect to its length L and height h as shape parameters to serve as a reference sensitivity solution to evaluate the accuracy of computational sensitivity analysis. Augarde and Deeks [17] elucidated the proper boundary conditions to impose when the analytic elasticity solution is used as a benchmark to evaluate convergence of adaptive finite element models. Here we adopt their reference frame in which the beam is cantilever at x=0 on the left with the parabolic load applied downward at x=L on the right. Their displacement solution, however, does not correspond to the one in [16] that allows shear deformation, which is used here as follows.

$$\begin{aligned} u(x,y) &= \frac{P}{EI}\left[\left(L-\frac{x}{2}\right)xy + \left((1+\nu)\frac{h^2}{4} - \kappa\right)y - \frac{(2+\nu)}{6}y^3\right] \\ v(x,y) &= \frac{-P}{EI}\left[\kappa x + \frac{Lx^2}{2} - \frac{x^3}{6} + \frac{\nu}{2}(L-x)y^2\right] \end{aligned} \tag{7}$$

where the beam has second area moment of inertia I= for a rectangular cross-section of unit depth b=1 with elastic modulus E and Poisson ratio ν, subject to parabolic transverse shear with total force P. This solution corresponds to a shear angle at the root of $P/(kG)$ with respect to the horizontal for shear reduction factor k=2/3 and shear modulus $G = \frac{E}{2(1+\nu)}$ and shear force effect factor $\kappa = \frac{EI}{kAG} = h^2(1+\nu)/4$. For the numerical results to follow the parameter values specified in [17] were used: h=2, L=8, P=2, E=1,000, κ=1.25, and ν=0.25. Boundary conditions at the root nodes of the finite element were imposed as enforced displacements in the finite element model for the analysis in accordance with Eqs. (7) at x=0.

$$\begin{Bmatrix} u(0,y) \\ v(0,y) \end{Bmatrix} = \begin{Bmatrix} \frac{P}{EI}\left[\left((1+\nu)\frac{h^2}{4} - \kappa\right)y - \left(\frac{2+\nu}{6}\right)y^3\right] \\ \frac{-P}{EI}\left(\frac{\nu}{2}\right)Ly^2 \end{Bmatrix} \tag{8}$$

Consistent nodal loads were applied for the following parabolic shear stress traction Φ_y at x=L.

$$\Phi_y(L,y) = \frac{3}{2}\left(\frac{-P}{bh}\right)\left[1 - \left(\frac{y}{c}\right)^2\right] \tag{9}$$

where c=$h/2$.

The sensitivity $\dot{\boldsymbol{g}}_e$ of the geometric boundary condition (8) is non-zero with respect to length L for the vertical root defection $v(0,y)$ and for both root deflections with respect to height h due to dependence on moment of inertia I. These were imposed as enforced displacements in the finite element model for the sensitivity solution.

$$\dot{\boldsymbol{g}}_{e,L} = \frac{D\boldsymbol{g}_e}{DL} = \begin{Bmatrix} \frac{Du(0,y)}{DL} \\ \frac{Dv(0,y)}{DL} \end{Bmatrix} = \begin{Bmatrix} \dot{u}(0,y) \\ \dot{v}(0,y) \end{Bmatrix} = \begin{Bmatrix} 0 \\ \frac{-P}{EI}\frac{\nu}{2}y^2 \end{Bmatrix} \tag{9}$$

The sensitivity load $\dot{\boldsymbol{g}}_n$ for the parabolic transverse shear at x=L is zero with respect to length L for constant total load P=2 in accordance with Eq. (9).

Figure 4 shows a course quadrilateral mesh for the Timoshenko beam and typical one-, two-, and 2.5-layer patches for the cantilever fixed end. The plot of true relative error demonstrates that the QUAD4 mesh achieves the expected second-order rate of convergence for tip deflection with respect to mesh refinement. The higher accuracy of the MSC Nastran reflects the higher quality of the MSC QUAD4 element.

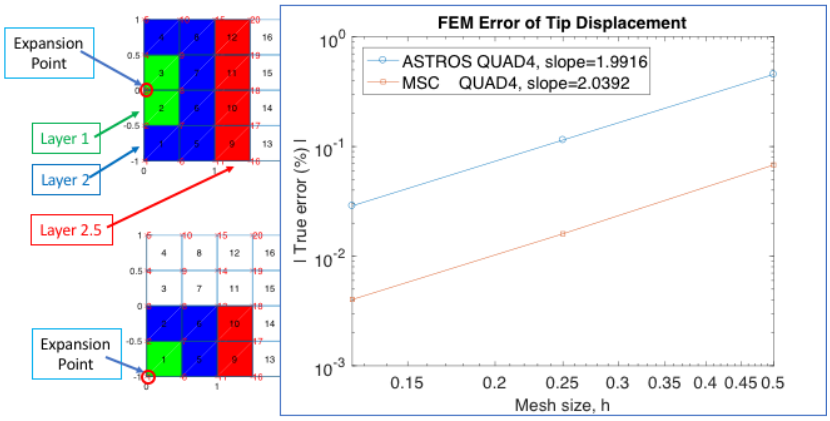

Figure 4. Timoshenko's beam tip deflection convergence (SGR patches shown on left)

Figure 5 shows convergence with respect to mesh size of axial normal strain, transverse normal strain, and transverse shear strain (spatial derivatives of displacement) as approximated by SGR for quadrilateral meshes for one-, two-, and 2.5-layer patches. Normal strains were reconstructed at the bottom left fixed corner of the mesh, as shown on the inset mesh on the left, whereas the shear strain was reconstructed at the neutral axis (centerline) of the fixed end, as shown on the inset mesh on the right of Fig. 5. One-layer patches achieve first-order rate of convergence. Two-layer and 2.5-layer patches match the second-order rate of convergence of the analysis, improving upon the accuracy of MSC Nastran element strains. Second-order accuracy of the FEM solution for displacements limit the accuracy achievable in reconstructing strains from FEM displacements using SGR.

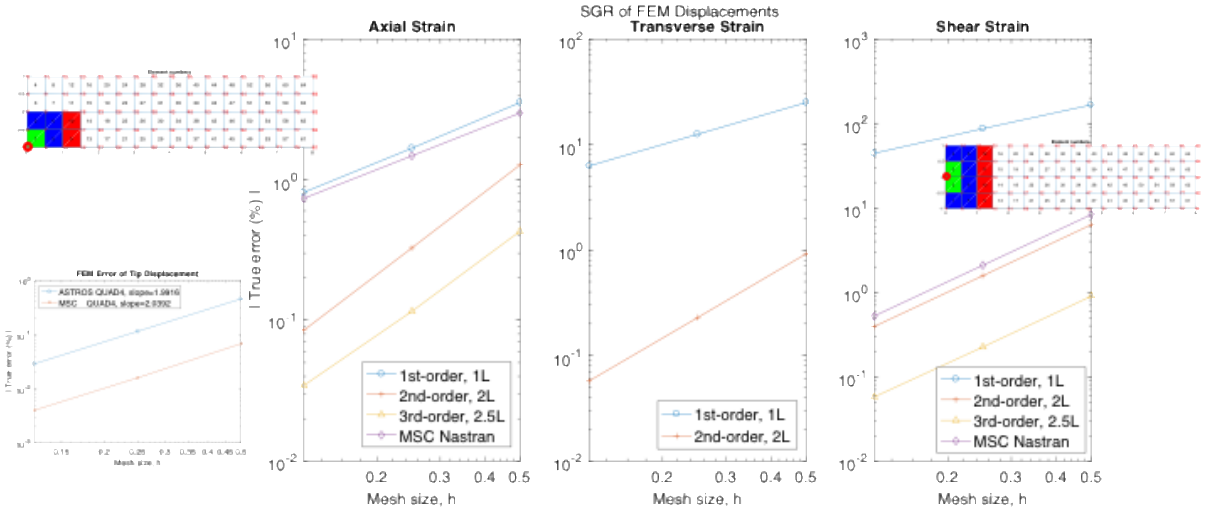

Figure 5. Timoshenko's beam SGR convergence for QUAD4 strain with 1-, 2-, and 3-layer patches (colored)

Figure 6 and 7 show convergence of true relative error with respect to mesh size of tip deflection, and axial normal strain, transverse normal strain, and transverse shear strain at the root, as approximated by SGR for unstructured triangular meshes generated by CAPS for one-, two-, and up to three-layer patches. SGR of normal strains are plotted for both corners of the beam root and a linear curve was fit to determine the rate-of-convergence slope. Transverse strain was reconstructed with SGR at the centerline (neutral axis) of the beam where it likewise is maximum in the cross-section.

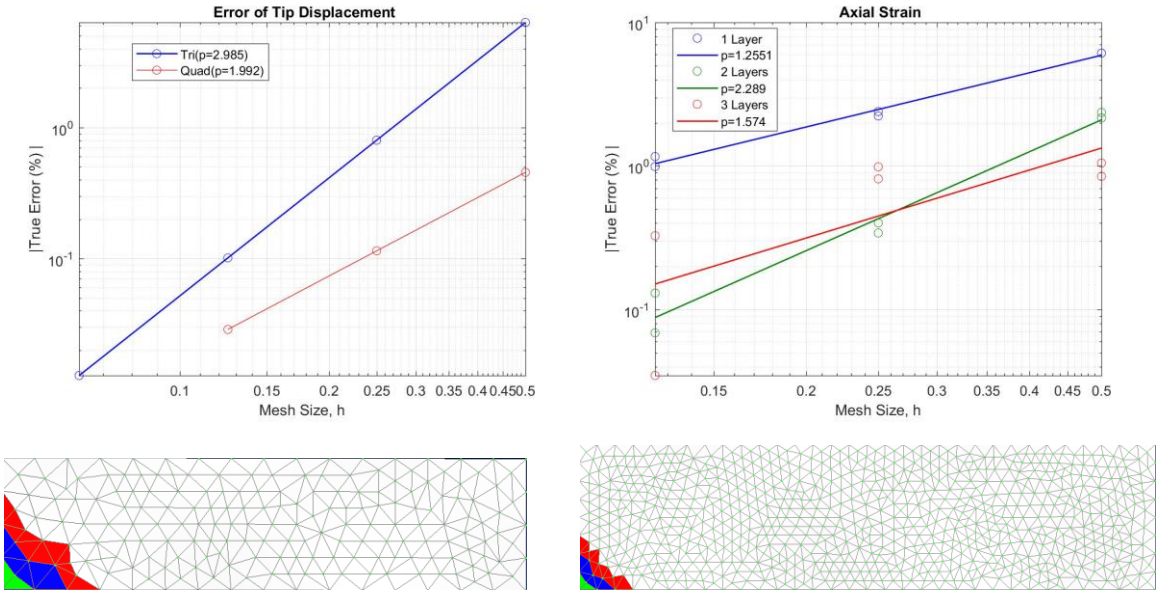

Figure 6. Timoshenko beam tip deflection (left) and SGR axial strain convergence (right) for TRIA3 strain with 1-, 2-, and 3-layer patches (colored elements) shown on coarse and medium CAPS meshes (bottom)

As expected, in Fig. 6 the linear triangular elements are less accurate for deflection than bilinear quadrilateral elements for a bending load, although the triangular rate of convergence is (unexpectedly) better. One-layer SGR patches achieve first-order rate of convergence for strains, as expected, mimicking the accuracy of strains computed from the finite elements themselves. Two-layer patches for axial strain and shear strain match the second-order rate of convergence of the analysis, improving upon the accuracy of the finite element strains. Although two-layer patches are more accurate for transverse normal strain at the beam root corners than one-layer patches, unfortunately they do not achieve the hoped-for second-order rate of convergence. Fortuitously, this spatial derivative does not enter the CSA calculation for shape derivative with respect to beam length. Unlike the quadrilateral meshes, three-

layer patches for the triangular meshes generally do not improve the accuracy of reconstructed strains relative to two-layer patches. Although third-order SGR is more accurate for axial strain of the coarsest mesh in Fig. 6, it deteriorates with mesh refinement due to superfluous data in the larger patch further from the expansion point. In Fig. 7 third-order SGR is again less accurate than second-order SGR for the coarse and medium meshes; however, its higher rate of convergence leads to it being marginally more accurate on the finest mesh, due to patch size become smaller and data from grid points furthest away from the expansion point are now closer to it. In summary, for axial strain the rate of convergence worsens for three-layer patches of triangular elements, whereas for transverse normal and shear strain the rate of convergence improves slightly, compensating for the worse bias in accuracy at these mesh sizes. The accuracy of SGR strains are evident in the CSA shape derivatives calculated from them, shown next.

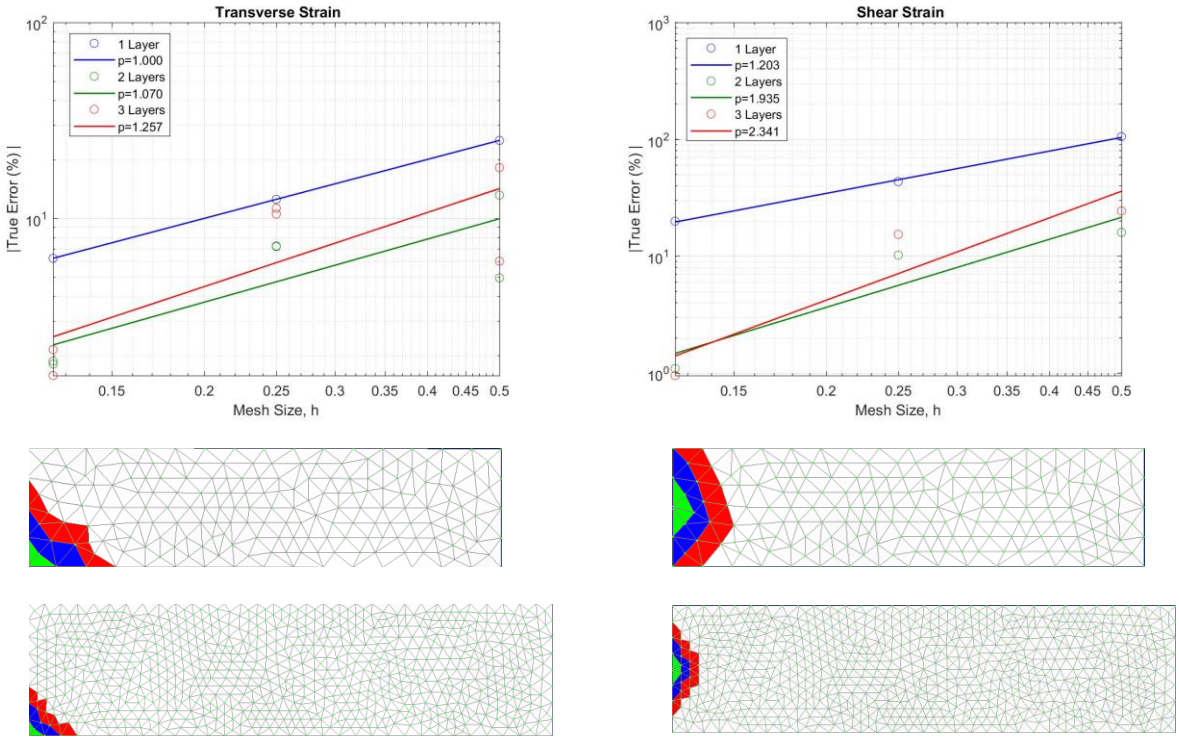

Figure 7. Timoshenko beam SGR transverse normal (left) and shear strain (right) convergence for TRIA3 strain with 1-, 2-, and 3-layer patches (colored elements) shown on coarse and medium CAPS meshes (bottom)

CSA results for shape derivatives of the Timoshenko beam tip displacement using the spatial derivatives estimated from SGR are presented in Fig. 8 for structured (QUAD4) and unstructured meshes (TRIA3).

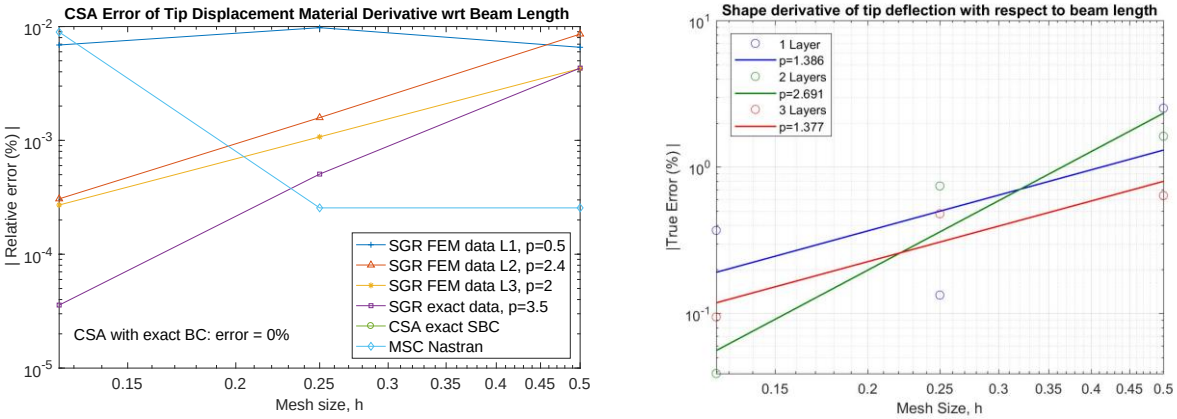

Figure 8. Timoshenko beam true relative error convergence of tip deflection shape derivative with respect to beam length for CAPS QUAD4 (left) and TRIA3 (right) meshes with 1-, 2-, and 3-layer patches

Unsurprisingly, as expected from prior results found in the literature, one-layer patches give inaccurate shape derivatives, not achieving even first-order rate of convergence for quadrilateral meshes. Two-layer patches used to reconstruct spatial derivatives from the FEM displacement results exceed the hoped-for second-order rate of convergence for both quadrilateral and triangular meshes. Rate of convergence worsens for three-layer patches, although they were slightly more accurate for the coarse triangular meshes. The markers labeled "SGR exact data" for which the rate of convergence exceed third order, were obtained by reconstructing spatial derivatives from the exact solution rather than from the FEM displacement data. Hence, this result demonstrates the limit of how accurate the CSA shape derivative could be, given the most accurate possible SGR for a given patch. The markers labeled "CSA exact SBC" do not appear on the plot because their error was below the precision of the printed results (effectively 0% relative error). They were computed using the exact sensitivity boundary conditions (SBC) known from Eq. (9). Thus, this result indicates that, if the SBC could be reconstructed with enough accuracy, then the FEM used to solve the discretized CSEs would give shape derivatives accurate to within the printed precision (six digits). For reference, the MSC Nastran shape derivative for its QUAD4 element are shown on the left plot of Fig. 8 to demonstrate that CSA sensitivity becomes more accurate with mesh refinement than the semi-analytic discrete shape derivative using a better QUAD4 finite element than the ASTROS QUAD4 element used for the CSA. Interestingly, the MSC Nastran shape derivative does not improve with mesh refinement, indeed worsening at the finest mesh, perhaps due the step-size choice for the finite-difference computation of the stiffness matrix sensitivity, which is avoided in CSA.

Three-Dimensional Solid Element Cantilever Beam Example

Six design variables originally were defined for the MSC Nastran solid element cantilever beam (Fig. 9). The first two design variables changed the height by moving the top face upward and the bottom face downward, respectively. The third and fourth design variables changed the linear taper of the top and bottom faces, respectively. The fifth and sixth design variables change the taper cubically for the top and bottom face, respectively. Corresponding sensitivity loads were applied as consistent nodal loads at the corresponding surface that moved (i.e., where the design velocity was non-zero on the boundary). CSA shape total (material) derivative results are plotted in

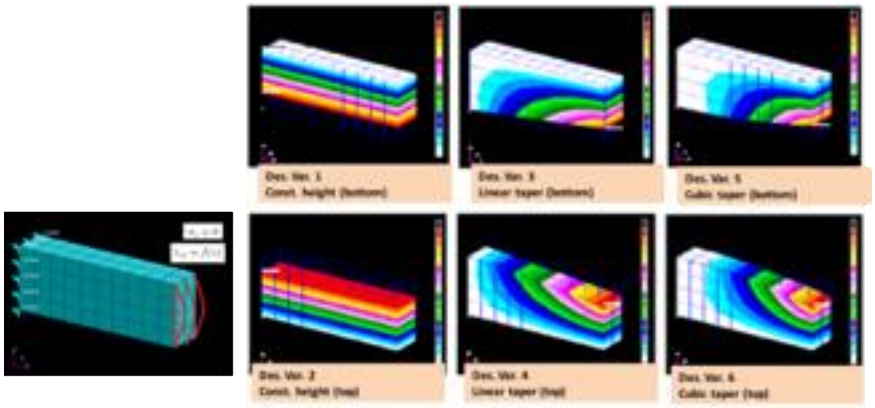

Figure 9. Solid element model for cantilever beam with height and taper shape design variables

Kulkarni [18] obtained the CSA results shown in Fig. 10, which the authors expect to duplicate using ASTROS with CAPS. Fig. 10 shows the solid-element cantilever beam's shape material derivative of transverse deflection along the span with respect to the six shape design variables. The CSA results obtained with second-order SGR patches agrees well with the MSC semi-analytic discrete shape derivative from Nastran Solution 200, as well as with the analytic (Airy stress solution) from the two-dimensional Timoshenko presented in the previous section.

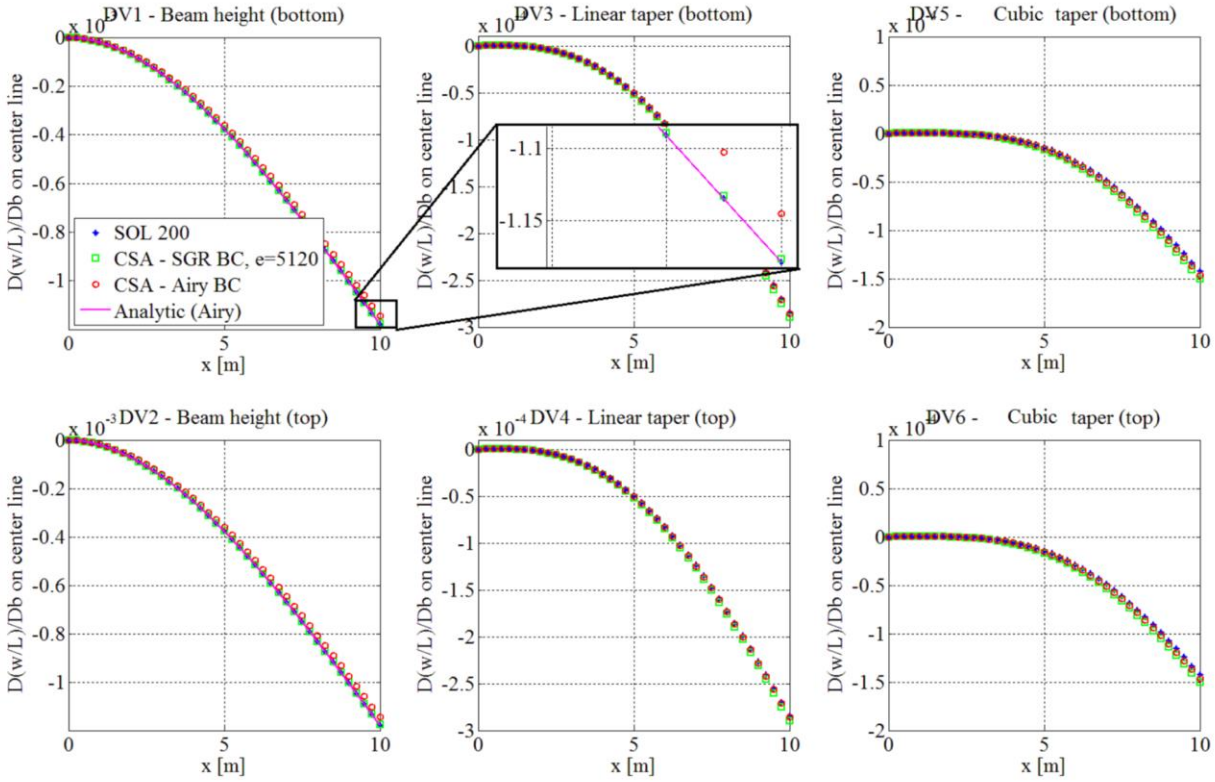

Figure 10. Shape total derivative of solid-element cantilever beam transverse deflection with respect to taper shape design variable [18]

Conclusion

Shape derivatives of structural response may be computed analytically using continuum sensitivity analysis. Boundary velocity CSA with SGR was implemented here in the ASTROS FEM program. SGR was implemented as an ASTROS module. SGR provided higher-accuracy reconstructed spatial derivatives (strains) and strain derivatives needed for accurate BV-CSA. Those spatial derivatives enter a convective term for sensitivity loads together with design velocity, which were obtained from the continuous geometric sensitivity in CAPS. Support for SGR patch definition was another capability added to CAPS. The resulting capability is a step toward generalizing BV-CSA in a nonintrusive manner. Future results demonstrate that NASTRAN FEM results may be post-processed by SGR in ASTROS. Together with design velocity from CAPS and the system stiffness matrix from NASTRAN, an analytical sensitivity will be available to compute shape derivatives of NASTRAN FEM results.

Acknowledgments

This material is based on research sponsored by the U.S. Air Force Office of Scientific Research (AFOSR). The U.S. Government is authorized to reproduce and distribute reprints for Governmental purposes notwithstanding any copyright notation thereon. Cleared for public release, Reference Number: RQ-18-1099. The authors gratefully acknowledge the support of AFOSR and the Program Officers for Computational Mathematics, Dr. Jean-Luc Cambier and Dr. Fariba Fahroo. The first author gratefully acknowledges the Air Force Research Laboratory Multidisciplinary Science and Technology Center for supporting the research sabbatical.

Appendix

A Python script generates the geometry, mesh, and ASTROS input file (Fig. A.1). The CAPS ASTROS AIM generates design velocities for shape design variables using standard NASTRAN DVGRID bulk data (Fig. A.2). Material derivatives of surface normal vectors are generated on newly defined SNORMDT bulk data entry (Fig. A.3). New input bulk data, such as the PATCHSET and PATCH2 bulk data entries shown in Fig. A.4, were created for ASTROS to pre-process patches and post-process FEM results to compute the SGR.

Figure A.1. pyCAPS AIM creates ASTROS or Nastran input data

```
# Set design variable
myAnalysis.setAnalysisVal("Design_Variable", ("xleft", {}))
#myAnalysis.setAnalysisVal("Design_Variable",  ("mThick", propertyDV))

# Set design constraints and responses
designConstraint1 = {"groupName" : "plate",
                     "responseType" : "STRESS",
                     "lowerBound" : -madeupium["yieldAllow"],
                     "upperBound" :  madeupium["yieldAllow"],}
# Set design constraint
myAnalysis.setAnalysisVal("Design_Constraint",[("stress", designConstraint1)])

# Set load
load = {"groupName" : "plate",
        "loadType" : "Pressure",
        "pressureForce" : 2.0}
# Set loads
myAnalysis.setAnalysisVal("Load", ("appliedPressure", load ))

# Set analysis
value = {"analysisType"       : "Static",
         "analysisConstraint"    : "BoundaryCondition",
         "analysisLoad"       : "appliedPressure",
         "analysisDesignConstraint" : "stress",
         "objectiveMinMax" : "MIN",
         "objectiveResponseType" : "WEIGHT"}
myAnalysis.setAnalysisVal("Analysis", ("Load", value ))

# Set analysis type
myAnalysis.setAnalysisVal("Analysis_Type", "StaticOpt");
#myAnalysis.setAnalysisVal("Analysis_Type", "Optimization")

# Run AIM pre-analysis
myAnalysis.aimPreAnalysis()
```

myProblem.loadCAPS("./csmData/plateBeam.csm")
#myAnalysis.setAnalysisVal("Quad_Mesh", True)

Figure A.2. *Design_Variable* generates DVGRID shape design variable input data

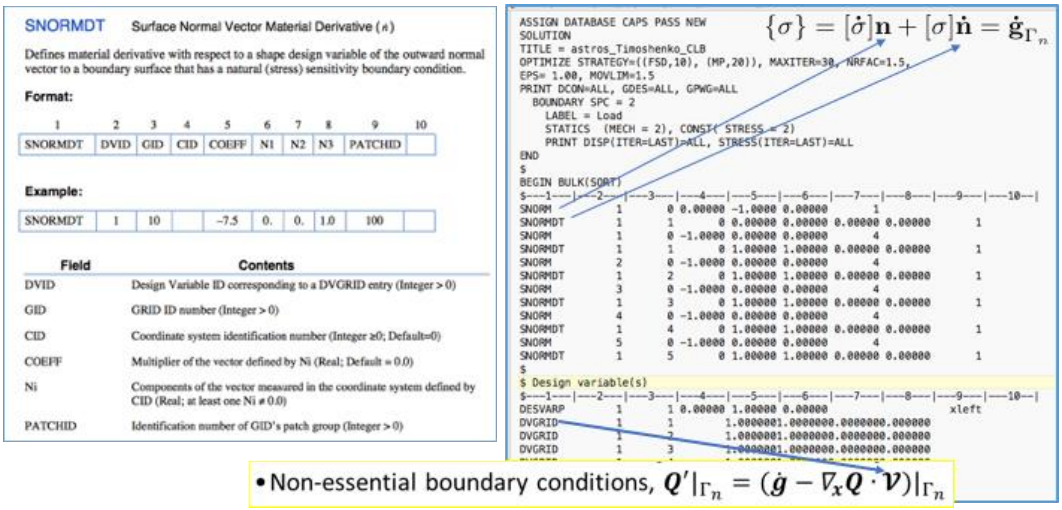

Figure A.3. SNORMDT surface normal derivative input for ASTROS CSA-SGR

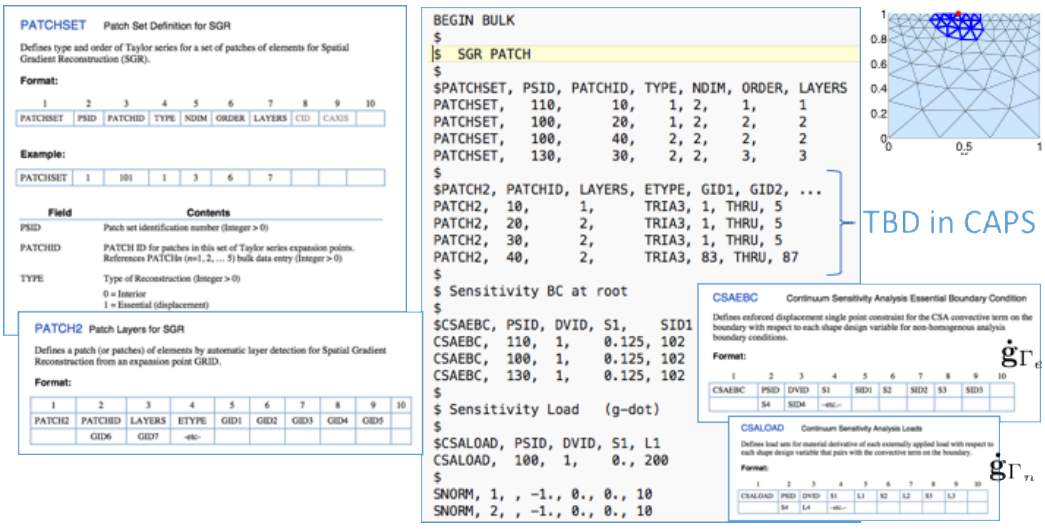

Figure A.4. SGR Patches in ASTROS

References

[1] Alyanak, E., Durscher, R., Haimes, R., Dannenhoffer, J., Bhagat, N. D., and Allison, D. L. "Multi-fidelity Geometry-centric Multi-disciplinary Analysis for Design," AIAA Modeling and Simulation Technologies Conference. American Institute of Aeronautics and Astronautics, 2016. doi: 0.2514/6.2016-4007

[2] Dannenhoffer, J., and Haimes, R. "Using Design-Parameter Sensitivities in Adjoint-Based Design Environments," 55th AIAA Aerospace Sciences Meeting. American Institute of Aeronautics and Astronautics, 2017. doi:10.2514/6.2017-0139

[3] Haimes, R., and Dannenhoffer, J. "EGADSlite: A Lightweight Geometry Kernel for HPC," 2018 AIAA Aerospace Sciences Meeting. American Institute of Aeronautics and Astronautics, 2018. doi:10.2514/6.2018-1401

[4] Neill, D. J., Johnson, E. H., and Canfield, R. "ASTROS—A Multidisciplinary Automated Structural Design Tool," *J. Aircraft* Vol. 27, No. 12, 1990, pp. 1021–1027. doi: 10.2514/3.45976

[5] Johnson, E., Chou, G. D., Zhang, S., Yu, X., Natarajan, S., and Reymond, M. MSC Nastran 2012 Design Sensitivity and Optimization User's Guide. Santa Ana, CA: MSC.Software Corporation, 2011

[6] Choi, K. K., and Kim, N. H. Structural sensitivity analysis and optimization. New York: Springer Science+Business Media, 2005.

[7] Liu, Shaobin; Canfield, Robert. A. (2013a), "Boundary Velocity Method for Continuum Shape Sensitivity of Nonlinear Fluid-Structure Interaction Problems," Journal of Fluids and Structures, Vol. 40, pp. 284–301, doi: 10.1016/j.jfluidstructs.2013.05.003

[8] Cross, David M. and Canfield, Robert A. (2014), "Local continuum shape sensitivity with spatial gradient reconstruction," Structural and Multidisciplinary Optimization, DOI 10.1007/s00158-014-1092-0, June 2014

[9] Zienkiewicz, O. C., and Zhu, J. Z. "The superconvergent patch recovery and a posteriori error estimates. Part 1: The recovery technique," International Journal for Numerical Methods in Engineering Vol. 33, No. 7, 1992, pp. 1331-1364. doi: 10.1002/nme.1620330702

[10] Canfield, Robert A., and David A. Sandler, "Continuum shape sensitivity analysis for aeroelastic gust using an arbitrary Lagrangian-Eulerian reference frame," Structural and Multidisciplinary Optimization, May 2018, Volume 57, Issue 5, pp 1871–1887. doi: 10.1007/s00158-018-1947-x.

[11] Cross, David M.; and Canfield, Robert A., "Local Continuum Shape Sensitivity with Spatial Gradient Reconstruction for Nonlinear Analysis," Structural and Multidisciplinary Optimization, April 2015, Volume 51, Issue 4, pp 849-865, doi: 10.1007/s00158-014-1178-8

[12] Cross, David M.; and Canfield, Robert A. "Convergence Study for the Local Continuum Sensitivity Method Using Spatial Gradient Reconstruction," AIAA Journal, Vol. 54, No. 3, March 2016, pp. 1050–1063, doi: 10.2514/1.J053800

[13] Kulkarni, Mandar D.; Cross, David M.; and Canfield, Robert A., "Discrete Adjoint Formulation for Continuum Sensitivity Analysis," AIAA Journal, Vol. 54, No. 2, February 2016, doi: 10.2514/6.2015-0138,

[14] Liu, Shaobin; and Canfield, Robert. A. (2013b), "Equivalence of Continuum and Discrete Analytic Sensitivity Methods for Nonlinear Differential Equations," Structural and Multidisciplinary Optimization, doi: 10.1007/s00158-013-0951-4 December 2013, Volume 48, Issue 6, pp. 1173–1188

[15] Liu, Shaobin; and Canfield, Robert A. (2016) "Two Forms of Continuum Shape Sensitivity Method for Fluid-Structure Interaction Problems," Journal of Fluids and Structures, Vol. 62, pp. 46–64, doi: 10.1016/j.jfluidstructs.2015.12.013

[16] Timoshenko, S., and Goodier, J., **Theory of Elasticity**, McGraw-Hill, 1951.

[17] Augarde, C. E., and Deeks, A. J. "The use of Timoshenko's exact solution for a cantilever beam in adaptive analysis," *Finite Elements in Analysis and Design* Vol. 44, No. 9, 2008, pp. 595-601. doi: 10.1016/j.finel.2008.01.010

[18] Kulkarni, Mandar D., "Continuum Sensitivity Analysis using Boundary Velocity Formulation for Shape Derivatives," PhD Dissertation, http://hdl.handle.net/10919/73057, August, 2016